Elastic relaxations associated with the $Pm\bar{3}m$–$R\bar{3}c$ transition in $LaAlO_3$: I. Single crystal elastic moduli at room temperature

2010 J. Phys.: Condens. Matter 22 035403

(http://iopscience.iop.org/0953-8984/22/3/035403)

J. Phys.: Condens. Matter **22** (2010) 035403 (11pp) doi:10.1088/0953-8984/22/3/035403

Elastic relaxations associated with the $Pm\bar{3}m$–$R\bar{3}c$ transition in $LaAlO_3$: I. Single crystal elastic moduli at room temperature

M A Carpenter[1], S V Sinogeikin[2], J D Bass[2], D L Lakshtanov[2,4] and S D Jacobsen[3]

[1] Department of Earth Sciences, University of Cambridge, Downing Street, Cambridge CB2 3EQ, UK
[2] Department of Geology, University of Illinois, Urbana, IL 61801, USA
[3] Department of Earth and Planetary Sciences, Northwestern University, Evanston, IL 60208, USA

E-mail: mc43@esc.cam.ac.uk

Received 1 August 2009, in final form 14 October 2009
Published 21 December 2009
Online at stacks.iop.org/JPhysCM/22/035403

Abstract
Values for all six independent components of the $\bar{3}m$ elastic modulus tensor of $LaAlO_3$ perovskite are reported. These were determined by means of Brillouin scattering measurements of acoustic velocities in single crystal plates cut parallel to (110) and (100), as defined with respect to the cubic parent structure, and by pure-mode longitudinal and transverse sound velocity measurements along [100], [110] and [111] directions using GHz pulse-echo ultrasonics. The crystals contained intimate intergrowths of twins arising from the $Pm\bar{3}m \leftrightarrow R\bar{3}c$ transition at higher temperature but, in combination with a careful analysis of twin orientation relationships, the two sets of data have allowed a unique solution to be obtained for individual twin components. The new data set represents an important contribution to the characterization of $LaAlO_3$ single crystals which are widely used as the substrate for a plethora of different thin films with technological applications.

1. Introduction

$LaAlO_3$ is currently one of the most important single crystal substrate materials for the growth of thin films with diverse physical, chemical and electronic properties. Some of the criteria involved in the choice of substrate material to support superconducting thin films were set out by Phillips (1996) and many of the earlier applications were for the cuprate superconductors, including $YBa_2Cu_3O_{7-\delta}$ (e.g., Simon *et al* 1988). $LaAlO_3$ can also be used in thin-film form itself, either intergrown with the superconductor (e.g., Lee *et al* 1990) or for its high-k dielectric properties on a Si substrate (e.g., Xiang *et al* 2003). More recently, $LaAlO_3$ single crystals have been used to support ferroelectric thin films such as $BaTiO_3$ (Zhu *et al* 2006) and $(Ba, Sr)TiO_3$ (Liu and Jiang 2006), manganite thin films for their electrical characteristics (e.g., Masuno *et al* 2004, Lehmann *et al* 2007) or other perovskite thin films with progressively more complex structures (e.g., Masuno *et al* 2006). This expanding list of applications has also resulted in a flurry of computational studies of structural, physical and defect properties (Peacock and Robertson 2002, Delugas *et al* 2005, Shevlin *et al* 2005, Xiong *et al* 2006, Luo and Wang 2008a, 2008b, Vali 2008). Given that many of the applications depend to some extent on elastic thin film–substrate interactions, it is surprising that there appear to have been no experimental determinations of the elastic moduli of $LaAlO_3$. The bulk modulus is known from high pressure equation of state measurements (Bouvier and Kreisel 2002, Zhao *et al* 2004), but the present authors have not been able to find values in the literature for the shear modulus or

[4] Present address: BP Labs, 200/55 Chertsey Road, Sunbury on Thames, TW16 7BP, UK.

for individual single crystal moduli. The bulk properties of $LaAlO_3$ have also become of interest from an earth sciences perspective since the discovery of superelastic behaviour under mechanical load due to the mobility of twin walls (Harrison and Redfern 2002, Harrison *et al* 2004b, 2004a). Elastic softening and anelastic dissipation associated with phase transitions could have implications for our understanding of the seismic properties of silicate perovskites in the lower mantle (Harrison and Redfern 2002, Walsh *et al* 2008). Against this general background, the specific objectives of the present study were to characterize the elastic properties of $LaAlO_3$ both at room temperature and at high temperatures through the $Pm\bar{3}m \leftrightarrow R\bar{3}c$ octahedral tilting transition which occurs near 820 K. In combination, data from different elasticity measurements provide a new and comprehensive view of the role of elastic relaxations associated with the transition which may also be more generally prevalent in perovskites. The underlying premise is that understanding the details of elastic softening and anelastic dissipation should enhance capabilities for engineering these materials in technological applications.

This paper is the first in a sequence of four on the elastic and acoustic dissipation properties of $LaAlO_3$. In paper I, values of the room temperature elastic modulus matrix are presented, as obtained by a combination of Brillouin scattering and GHz pulse-echo ultrasonic techniques. Because single crystals prepared at high temperatures contain intimate intergrowths of transformation twins which develop during cooling through the $Pm\bar{3}m \leftrightarrow R\bar{3}c$ transition, a rather careful analysis of the possible twin orientations has been required. In paper II (Carpenter *et al* 2010c) Brillouin data obtained at high temperatures up to ~1000 K are presented. These allow a complete calibration of the Landau free energy expansion that is expected to provide a quantitative description of changes in physical properties through the phase transition. The observation of significant quasi-elastic scattering in a temperature interval of ~100 K below the transition point implies the involvement of a significant dynamical component in the transition. In papers III (Carpenter *et al* 2010a) and IV (Carpenter *et al* 2010b), elastic and anelastic properties determined by resonant ultrasound spectroscopy are described. These further highlight the importance of dynamical relaxation processes in determining the response of $LaAlO_3$ to mechanical stress. It should be noted that the recent spectroscopic study of Sathe and Dubey (2007) provides evidence that the local symmetry of rhombohedral $LaAlO_3$ could be $R\bar{3}$ or $R3c$ instead of $R\bar{3}c$. The data presented here and in Carpenter *et al* (2010c, 2010a) provide an internally consistent picture based on $R\bar{3}c$. There is some anelastic dissipation behaviour at low temperatures which could be understood in terms of such a local symmetry reduction, but this is considered in more detail in Carpenter *et al* (2010b).

2. Sample preparation

Single crystals of $LaAlO_3$ used in the present study were prepared together as a batch from a larger pale pink crystal purchased from Crystal Gmbh (Berlin) that had been grown by the Czochralski method. Some of this sample was also used for neutron diffraction, heat capacity, Raman spectroscopy and optical retardation measurements by Hayward *et al* (2005). Crystal Gmbh provided the single crystals used by Bueble *et al* (1998), Chrosch and Salje (1999), Hayward *et al* (2002) and Harrison and Redfern (2002), and it is therefore assumed that the data in all these studies were collected from $LaAlO_3$ with essentially the same physical and chemical properties.

Laue back reflection x-ray diffraction was used to orient the large starting crystal so that plates parallel to (100) and (110) (±~1°), defined with respect to cubic reference axes, could be sawn from it with a fine annular diamond saw lubricated with paraffin. $LaAlO_3$ is rhombohedral at room temperature but the distortion from cubic lattice geometry is so small that a cubic reference system can be used without loss of precision in this context. The plates were doubly polished to a thickness of 190 ± 1 μm and sliced into smaller pieces. (100) plates had final dimensions of ~1 mm × 1 mm in plan view, with edges parallel to [001] and [010]. (110) plates had dimensions of ~1 mm × 0.5 mm, with the long dimension parallel to [001] and the short edge parallel to $[1\bar{1}0]$. Two further plates were prepared for GHz pulse-echo ultrasonic measurements. A (110) plate was polished down to 100±1 μm and cut into 250 × 250 μm squares. A plate with polished faces parallel to (111) was cored from a piece of the original $LaAlO_3$ crystal, using an x-ray precession camera to confirm the orientation. This plate had a diameter of 210 μm and a thickness of 95 ± 1 μm.

Using $a = 5.365\,40(7)$, $c = 13.1126(2)$ Å for the trigonal unit cell at room temperature, as obtained by Hayward *et al* (2005), together with assumed ideal stoichiometry and a molecular weight of 213.89 g, gives a theoretical density of 6.52 g cm^{-3}. The density of a large piece of the original sample was checked by the Archimedes method using distilled water, and was found to be 6.526 ± 0.003 g cm^{-3}, with the principal uncertainty being propagated from a value of 0.998±0.005 g cm^{-3} for the density of distilled water at 20 °C. In all calculations of the moduli, the theoretical density has been used.

3. Characterization of twin orientations

Single crystals of $LaAlO_3$ typically contain abundant transformation twins which develop during cooling through the $Pm\bar{3}m \leftrightarrow R\bar{3}c$ transition. As described in detail by Bueble *et al* (1998) and Harrison and Redfern (2002), the $\bar{3}$ axis of the rhombohedral phase (=$[001]_{trigonal}$) can be aligned parallel to [111], $[1\bar{1}1]$, $[\bar{1}11]$ or $[\bar{1}\bar{1}1]$ of the cubic parent phase and there are six possible pairs of twin planes separating these domains. The four distinct domains are referred to below in terms of their unique directions, and the possible twin relationships between them are illustrated in figure 1.

Examination between crossed polars in a petrographic microscope revealed that the (110) plate used for the Brillouin scattering experiment contained a small number of twins. Twin walls with traces parallel to $[1\bar{1}0]$ were present at the start. These disappeared after the first heating and cooling cycle to temperatures above the $Pm\bar{3}m \leftrightarrow R\bar{3}c$ transition point, leaving visible twin walls only parallel to [001]. Subsequent

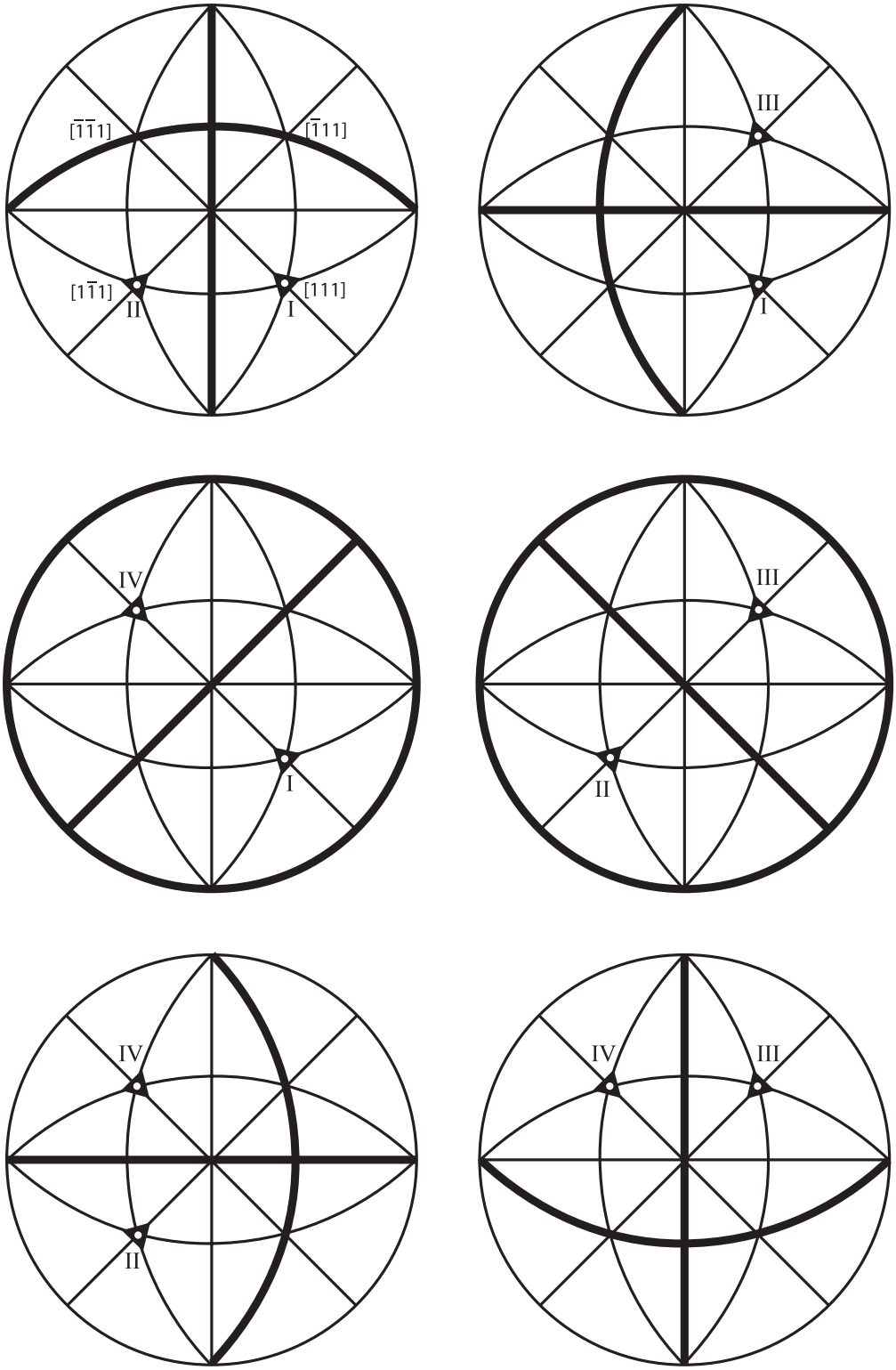

Figure 1. Possible domain orientations and twin wall orientations in a crystal with $\bar{3}m$ symmetry following a phase transition involving the symmetry change $m\bar{3}m \rightarrow \bar{3}m$. Following Bueble *et al* (1998), domains with their threefold axes parallel to [111], [1$\bar{1}$1], [$\bar{1}$11] or [$\bar{1}\bar{1}$1] are referred to below as domain states I, II, III and IV respectively. Twin wall orientations for different pairs of twin domains are shown in bold. (See, also, Harrison and Redfern 2002.)

checks of the optical orientation showed that the central portion of the crystal had permitted vibration directions parallel to the edges of the crystal, i.e. parallel to [001] and [1$\bar{1}$0]. Outer portions, beyond the [001] traces, had permitted vibration directions inclined at a steep angle to [1$\bar{1}$0] and [001]. These observations are consistent with the presence of [111] and/or [$\bar{1}\bar{1}$1] domains in the central region from which Brillouin spectra and GHz ultrasonic velocities were obtained (figure 2),

and [$\bar{1}11$] or [$1\bar{1}1$] domains at the edges. [111] and [$\bar{1}\bar{1}1$] domains coexist across (110) and (001) twin planes (figure 1; Bueble *et al* 1998), so it is possible that both domains were present, with twin walls parallel to the faces of the plate. Examination of the plate in a petrographic microscope fitted with a universal stage, after completion of the high temperature experiments described in Carpenter *et al* (2010c), revealed the presence of at least one twin wall parallel to (110). The distribution of symmetry elements of point group symmetry $\bar{3}m$ for [111] and [$\bar{1}\bar{1}1$] domains is illustrated in figure 2 to show that (110) is a crystallographic plane which contains the same symmetry elements in both twins. Brillouin spectra from this plate, therefore, should not show evidence of twinning even if the scattered light came from different domains across one or more (110) twin walls.

The square (100) plate used for Brillouin scattering contained multiple lamellar twins with twin wall traces aligned predominantly parallel to only one edge. Permitted light vibration directions were parallel to the diagonals of the plate, i.e. parallel to [011] and [$0\bar{1}1$]. The fine spacing between walls ensured that the laser beam sampled acoustic phonons from at least two different twin domains. The precise combination of twins is not important, however, because only two distinct crystallographic planes could be present. These have [011] parallel to a diad and [$0\bar{1}1$] within a mirror plane or the diad parallel to [$0\bar{1}1$] and [011] within the mirror plane (see figure 2, for example). [010] and [100] directions would correspond to the same crystallographic direction for any of the four possible twin domains. It is expected therefore that the Brillouin spectra should show peaks from acoustic phonons corresponding to a maximum of two discrete twin orientations, irrespective of which particular combination of twins is actually being sampled.

The disc cut perpendicular to cubic [111] contained a complex pattern of twins which was not analysed in detail. It is presumed simply to have contained different proportions of some or all of the four possible twin domains.

4. Cubic and trigonal reference systems

Analysis of elastic modulus variations across the $Pm\bar{3}m \leftrightarrow R\bar{3}c$ transition requires the use of cubic reference axes for the $R\bar{3}c$ structure, while extraction of the moduli from Brillouin data for this phase required the use of a trigonal reference system. The two different reference axes used here are shown in figure 3 and expressions for the relationship between moduli of both systems, obtained by standard transformation of axes for a fourth rank tensor, are listed in table 1. Non-zero elastic moduli for the trigonal reference axes are $C_{11T} = C_{22T}$, C_{33T}, C_{12T}, $C_{13T} = C_{23T}$, $C_{14T} = -C_{24T} = C_{56T}$, $C_{44T} = C_{55T}$, $C_{66T} = \frac{1}{2}(C_{11T} - C_{12T})$ (Nye 1985). Non-zero moduli for the trigonal crystal expressed in terms of cubic reference axes are $C_{11} = C_{22} = C_{33}$, $C_{12} = C_{13} = C_{23}$, $C_{44} = C_{55} = C_{66}$, $C_{46} = C_{45} = C_{56}$, $C_{36} = C_{14} = C_{25}$, $C_{24} = C_{15} = C_{34} = C_{35} = C_{26} = C_{16}$.

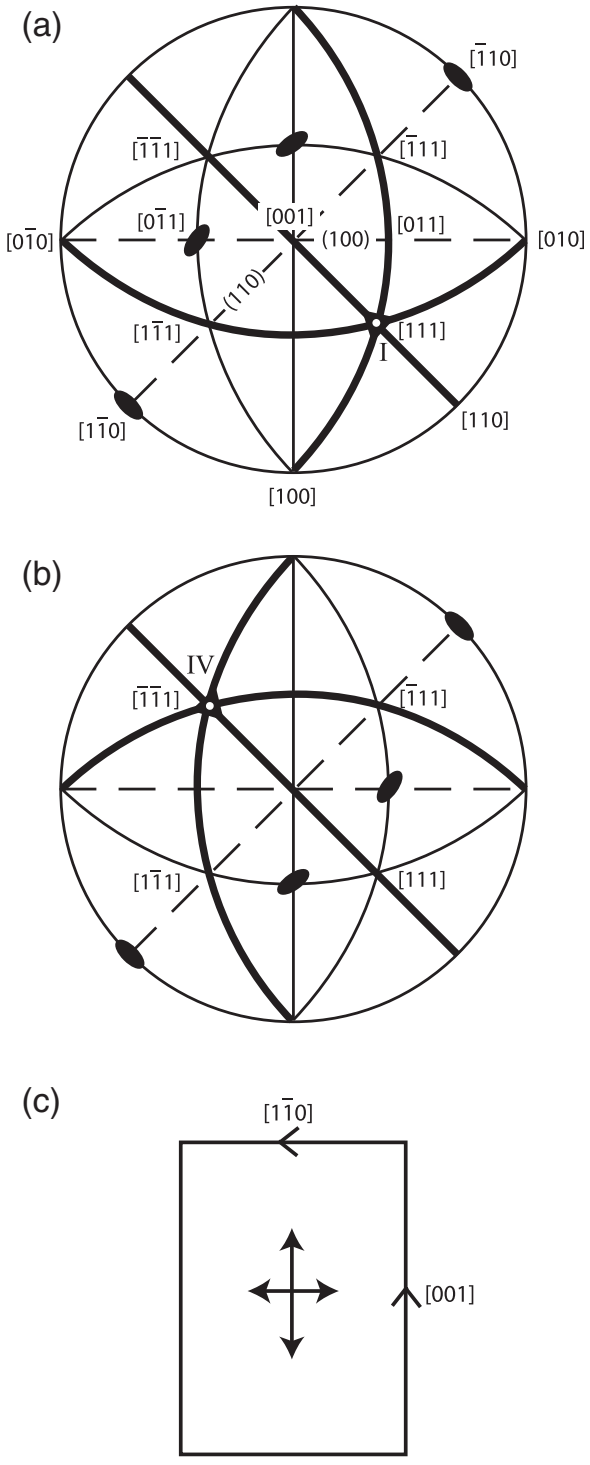

Figure 2. Orientation of twin domains in the (110) plates used for Brillouin scattering and GHz pulse-echo ultrasonic measurements, as deduced from observations in a petrographic microscope. Domains I (a) and IV (b) could coexist across a (110) twin plane and not be distinguished in the (110) plate. Permitted light vibration directions of the two domains (shown as double headed arrows) would correspond to the same section of the optical indicatrix and would be superimposed in the orientation shown in (c). Symmetry elements for the two domains are shown, with mirror planes in bold. The orientations of (110) and (100) plates are shown as broken lines. Note that [011] and [$0\bar{1}1$] of the (100) plate can only be parallel to a diad or lie within a mirror plane for any combination of twin domains shown in figure 1.

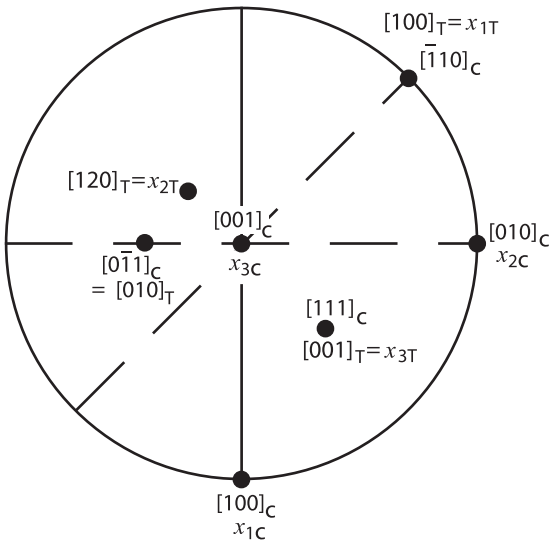

Figure 3. Orientation relationships used to describe single crystal elastic moduli of $\bar{3}m$ crystals for conventional reference axes of a trigonal system (Nye 1985; here labelled x_{1T}, x_{2T}, x_{3T}) and for cubic reference axes (x_1, x_2, x_3). Crystallographic directions in the two reference systems are indicated by subscripts T (trigonal) and C (cubic).

5. Experimental methods

5.1. GHz pulse-echo ultrasonics

Ultrasonic pulse-echo methods in the 1–2 GHz frequency range were developed to measure compressional (Spetzler *et al* 1993) and shear wave (Jacobsen *et al* 2002) acoustic travel times in sub-millimetre sized single crystals. A review of the technique is given by Jacobsen *et al* (2005), which has also been applied to study single crystal elasticity of opaque materials such as $Fe_{1-x}O$ at high pressures (Kantor *et al* 2004). Thin-film ZnO transducers are sputtered onto single crystal sapphire substrates, which act as buffer rods to deliver <100 ns tone bursts of the 1–2 GHz carrier frequency to the bonded sample in a microwave delay-line arrangement. By emitting two tone bursts with appropriate delay, the amplitude of overlapping pulses from the near and far-end of the sample is measured as the frequency varies to produce an acoustic interferogram with maxima and minima corresponding to integer and half-integer wavelengths in the round-trip distance through the sample. With acoustic velocities in the 3–10 km s^{-1} range, corresponding wavelengths at 1 GHz are 3–10 μm.

GHz ultrasonic measurements were carried out on (100), (110), and (111) plates of the $LaAlO_3$ material measuring 95–190 μm thick. Longitudinal velocities in the [100], [110], and [111] directions are reported in table 2, along with a transverse wave velocity in the [110] direction polarized [1$\bar{1}$0] vector. All GHz measurements were conducted in the 1–1.6 GHz frequency range. Because the travel times are determined with a precision of a few parts in 10^4, errors in the reported velocities are dominated by uncertainties in the crystal plate thickness, determined by mechanical micrometre measurements with nominal ± 1 μm accuracy. For this reason, an optical displacement interferometer is under construction for more precise sample thickness measurements. The current setup leads to uncertainties of a few GPa in 100.

Table 1. Expressions for single crystal elastic moduli referred to a trigonal reference system, C_{ikT}, in terms of moduli referred to a cubic reference system, C_{ik}. Orientation relationships between reference axes for the two systems are shown in figure 3.

$$C_{11T} = C_{22T} = \tfrac{1}{2}C_{11} + \tfrac{1}{2}C_{12} + C_{44} - 2C_{24}$$
$$C_{12T} = \tfrac{1}{3}(\tfrac{1}{2}C_{11} + \tfrac{5}{2}C_{12} - C_{44} - 2C_{24} - 4C_{36} + 4C_{46})$$
$$C_{33T} = \tfrac{1}{3}(C_{11} + 2C_{12} + 4C_{44} + 8C_{24} + 4C_{36} + 8C_{46})$$
$$C_{13T} = C_{23T} = \tfrac{1}{3}(C_{11} + 2C_{12} - 2C_{44} + 2C_{24} + C_{36} - 4C_{46})$$
$$C_{14T} = -C_{24T} = C_{56T} = \tfrac{1}{3\sqrt{2}}(-C_{11} + C_{12} + 2C_{44} + C_{24} - C_{36} - 2C_{46})$$
$$C_{44T} = C_{55T} = \tfrac{1}{3}(C_{11} - C_{12} + C_{44} + 2C_{24} - 2C_{36} - C_{46})$$
$$C_{66T} = \tfrac{1}{2}(C_{11T} - C_{12T})$$

Measurements were carried out by bonding the crystals to separate P- and S-wave buffer rods using an uncured UV-epoxy for P-wave measurements, and superglue adhesive for the S-wave measurement. Adding a few grams of weight to the sample contact and gliding the sample across the buffer rod tip in circular motions brings the bond thickness to <1 μm. Therefore, no bond correction was applied to the current measurements. The acoustic wavefield at GHz frequencies is approximately equal to the active transducer diameter of 200 μm. Care was taken to place the acoustic probe between twin walls to obtain measurements within an individual twin domain, as viewed through a reflected and transmitted light zoom microscope.

5.2. Brillouin spectroscopy

For Brillouin scattering experiments, the (110) and (100) $LaAlO_3$ plates were held within 350 μm thick pieces of Pt foil from which holes had been cut to match the shape of the crystals. The (110) plate was held in place during loading into the furnace by a small quantity of 'Resbond 940' ceramic cement placed at both ends and cured for 10 min at ~100 °C. It is likely that the cement cracked during the first heating runs described in Carpenter *et al* (2010c), so that it would not have provided a source of stress on the crystal. The (100) plate sat freely within the space cut through the Pt foil.

The Brillouin spectrometer used for data collection has been described elsewhere (Sinogeikin *et al* 1998, Palko *et al* 2002, Schilling *et al* 2003). In all experiments, an 80° symmetric scattering geometry was utilized in order to minimize effects of the refractive index of the sample on the observed Brillouin shift, $\Delta\omega$. Velocities, V, of acoustic phonons are calculated according to

$$V = \frac{\Delta\omega\lambda}{2\sin(\theta/2)}, \qquad (1)$$

with $\theta = 80°$. A polarizer was placed in the path of the incoming beam but there was no analyser in the path of the outgoing beam, so that longitudinal and shear waves could be obtained simultaneously.

Room temperature data were collected for directions spaced by 15° round 180° of the chi circle, i.e. within the plane

Table 2. Velocity and elastic modulus data obtained by GHz pulse-echo ultrasonics at room temperature (density = 6.52 g cm^{-3}; frequency range 1–1.4 GHz for expt. no. 4, 5, 1–1.6 GHz for expt. no. 17, 1–1.5 GHz for expt. no. 11). The 'equivalent Brillouin values' are calculated values based on the best fit set of moduli given in table 4.

Expt. no.	Plate	Orientation	Mode	Thickness (m)	Traveltime (s)	Velocity (m s^{-1})	ρv^2 (GPa)	Cubic elastic constant combination	Equivalent Brillouin value (GPa)
5	(110)	[110]	LA	1.90×10^{-4}	$4.801 \times 10^{-8} \pm 7.05 \times 10^{-12}$	7915 ± 43	408 ± 4	$\frac{1}{2}(C_{11}+C_{12}+2C_{44})$	397.3
4	(100)	[100]	LA	1.90×10^{-4}	$5.651 \times 10^{-8} \pm 3.18 \times 10^{-11}$	6724 ± 39	295 ± 3	C_{11}	289.8
17	(111)	[111]	LA	9.5×10^{-5}	$2.390 \times 10^{-8} \pm 3.14 \times 10^{-11}$	7950 ± 94	412 ± 10	$\frac{1}{3}(C_{11}+4C_{44}+2C_{12})$	[111]—411.2 [$\bar{1}$11]—390.5
11	(110)	[110]	TA, p[1$\bar{1}$0]	1.00×10^{-4}	$6.394 \times 10^{-8} \pm 1.24 \times 10^{-11}$	3128 ± 32	64 ± 1	$\frac{1}{2}(C_{11}-C_{12})$	68.3

Table 3. Elastic modulus combinations for LA- and TA-waves travelling in selected crystallographic directions through twin domains of type I (unique axis ∥ [111]) of a crystal with crystal class symmetry $\bar{3}m$ (see figure 2(a)). All the Miller indices and elastic moduli refer to cubic reference axes. Values for these combinations of moduli calculated using the 'best fit' room temperature values listed in table 4 are also given.

Direction	$Pm\bar{3}m$	$R\bar{3}c$	Calculated value (GPa)
[111]	LA: $\frac{1}{3}(C_{11}+4C_{44}+2C_{12})$ TA_1, TA_2: $\frac{1}{3}(C_{11}-C_{12}+C_{44})$	LA: $\frac{1}{3}(C_{11}+4C_{44}+8C_{24}+8C_{46}+4C_{36}+2C_{12})$ TA_1, TA_2: $\frac{1}{3}(C_{11}-C_{12}+2C_{24}-2C_{36}+C_{44}-C_{46})$	LA: 411.2 TA_1: 120.5 TA_2: 120.5
[$\bar{1}$11], [1$\bar{1}$1], [11$\bar{1}$]	LA: $\frac{1}{3}(C_{11}+4C_{44}+2C_{12})$	LA: $\frac{1}{6}(2C_{11}+C_{12}-2C_{24}-2C_{36}+5C_{44}-C_{46}+[9C_{12}^2-20C_{12}C_{24}+68C_{24}^2-4C_{12}C_{36}-24C_{24}C_{36}+4C_{36}^2+18C_{12}C_{44}-20C_{24}C_{44}-4C_{36}C_{44}+9C_{44}^2-26C_{12}C_{46}-28C_{24}C_{46}+20C_{36}C_{46}-26C_{44}C_{46}+33C_{46}^2]^{\frac{1}{2}})$	LA: 390.5
	TA_1, TA_2: $\frac{1}{3}(C_{11}-C_{12}+C_{44})$	TA_1: $\frac{1}{3}(C_{11}-C_{12}-2C_{24}+2C_{36}+C_{44}-C_{46})$ TA_2: $\frac{1}{6}(2C_{11}+C_{12}-2C_{24}-2C_{36}+5C_{44}-C_{46}-[9C_{12}^2-20C_{12}C_{24}+68C_{24}^2-4C_{12}C_{36}-24C_{24}C_{36}+4C_{36}^2+18C_{12}C_{44}-20C_{24}C_{44}-4C_{36}C_{44}+9C_{44}^2-26C_{12}C_{46}-28C_{24}C_{46}+20C_{36}C_{46}-26C_{44}C_{46}+33C_{46}^2]^{\frac{1}{2}})$	TA_1: 104.2 TA_2: 67.2
[1$\bar{1}$0], [0$\bar{1}$1], [$\bar{1}$01] (parallel to the diad)	P: $\frac{1}{2}(C_{11}+C_{12}+2C_{44})$	LA: $\frac{1}{2}(C_{11}+C_{12}-4C_{24}+2C_{44})$	LA: 337.3
	TA_1: C_{44}	TA_1: $\frac{1}{4}(C_{11}-C_{12}+2C_{44}-2C_{46}+[((-C_{11}+C_{12}-2C_{44}+2C_{46})^2-8(-C_{24}^2+2C_{24}C_{36}-C_{36}^2+C_{11}C_{44}-C_{12}C_{44}-C_{11}C_{46}+C_{12}C_{46}))]^{\frac{1}{2}})$	TA_1: 154.4
	TA_2: $\frac{1}{2}(C_{11}-C_{12})$	TA_2: $\frac{1}{4}(C_{11}-C_{12}+2C_{44}-2C_{46}-[(-C_{11}+C_{12}-2C_{44}+2C_{46})^2-8(-C_{24}^2+2C_{24}C_{36}-C_{36}^2+C_{11}C_{44}-C_{12}C_{44}-C_{11}C_{46}+C_{12}C_{46})]^{\frac{1}{2}})$	TA_2: 59.0
[110], [101], [011] (within mirror plane)	LA: $\frac{1}{2}(C_{11}+C_{12}+2C_{44})$	LA: $\frac{1}{4}(C_{11}+C_{12}+4C_{24}+4C_{44}+2C_{46}+[C_{11}^2+2C_{11}C_{12}+C_{12}^2+8C_{11}C_{24}+8C_{12}C_{24}+24C_{24}^2+16C_{24}C_{36}+8C_{36}^2-4C_{11}C_{46}-4C_{12}C_{46}+16C_{24}C_{46}+32C_{36}C_{46}+36C_{46}^2]^{\frac{1}{2}})$	LA: 397.3
	TA_1: C_{44}	TA_1: $\frac{1}{4}(C_{11}+C_{12}+4C_{24}+4C_{44}+2C_{46}-[C_{11}^2+2C_{11}C_{12}+C_{12}^2+8C_{11}C_{24}+8C_{12}C_{24}+24C_{24}^2+16C_{24}C_{36}+8C_{36}^2-4C_{11}C_{46}-4C_{12}C_{46}+16C_{24}C_{46}+32C_{36}C_{46}+36C_{46}^2]^{\frac{1}{2}})$	TA_1: 152.9
	TA_2: $\frac{1}{2}(C_{11}-C_{12})$	TA_2: $\frac{1}{2}(C_{11}-C_{12})$	TA_2: 68.3
[100], [010], [001]	LA: C_{11}	LA: $\frac{1}{2}(C_{11}+C_{44}+C_{46}+[C_{11}^2+8C_{24}^2-2C_{11}C_{44}+C_{44}^2-2C_{11}C_{46}+2C_{44}C_{46}+C_{46}^2]^{\frac{1}{2}})$	LA: 289.8
	TA_1, TA_2: C_{44}	TA_1: $(C_{44}-C_{46})$ TA_2: $\frac{1}{2}(C_{11}+C_{44}+C_{46}-[C_{11}^2+8C_{24}^2-2C_{11}C_{44}+C_{44}^2-2C_{11}C_{46}+2C_{44}C_{46}+C_{46}^2]^{\frac{1}{2}})$	TA_1: 145.1 TA_2: 149.6

Table 4. Elastic moduli for $LaAlO_3$ at room temperature, as obtained by fitting to LA, TA_1 and TA_2 velocities in spectra from the (100) and (110) plates combined, including the weak extra peaks in spectra from the (100) plate ($\rho = 6.52$ g cm^{-3}). The single crystal data are given for trigonal and cubic reference systems illustrated in figure 3. Bulk elastic moduli are Voigt–Reuss–Hill values obtained in the usual way from single crystal data. Estimated uncertainties propagated from the fitting are ±~1% for C_{11T}, C_{33T}, C_{44T} and ±2–3% for C_{12T}, C_{13T}, C_{14T}.

Trigonal ref. system (GPa)	Cubic ref. system (GPa)	Bulk (GPa)
$C_{11T} = 337.2$	$C_{11} = 286.5$	$K_V = 195.5$
$C_{12T} = 151.5$	$C_{12} = 150.0$	$K_R = 195.4$
$C_{33T} = 411.3$	$C_{44} = 149.0$	$K_H = 195.5$
$C_{13T} = 92.7$	$C_{46} = 3.9$	$G_V = 116.7$
$C_{44T} = 120.6$	$C_{36} = -25.0$	$G_R = 93.9$
$C_{14T} = 45.7$	$C_{24} = 15.0$	$G_H = 105.3$

of the plate. From the resulting pattern of velocities, prominent symmetry directions were located to within ±1° ([$\bar{1}$10] for the (110) plate and [001], [011], [0$\bar{1}$1] for the (100) plate). Each spectrum was an accumulation of ~180–1600 frequency scans of ~0.5 s (0.5 ms per channel, 1024 channels). For direct comparison between spectra, intensities have been rescaled to the equivalent of 500 scans per spectrum.

Complete sets of elastic moduli at room temperature were obtained by matching observed and calculated velocities of the longitudinal acoustic (LA) and transverse acoustic (TA) modes using in-house software and reference axes for the trigonal system (figure 3), in which $(110)_{cubic}$ becomes $(0\sqrt{2}1)_{trigonal}$ and $(100)_{cubic}$ becomes $(\sqrt{3}\bar{1}\sqrt{2})_{trigonal}$. Acoustic phonon velocities were converted to moduli, C, for each direction according to $C = \rho V^2$, where the density, ρ, was taken to be 6.52 g cm^{-3}.

6. Results

6.1. GHz pulse-echo ultrasonics

Travel times were obtained for compressional waves through (110), (100) and (111) plates. Taking into account the analysis of twin orientations given above, the travel direction through the (110) plate was [110]. This should be the same crystallographic direction in both orientations of [111] and [$\bar{1}\bar{1}$1] twins sharing (110) twin planes within the plane of the plate (figure 2). Twin walls in $LaAlO_3$ move readily under stress and the load of the lever arm of the GHz probe caused a complex pattern of multiple twinning to develop in the (100) plate. Velocities parallel to [100], [010] and [001] directions for all possible twin orientations should be determined by the same combination of moduli, however, and the travel direction can be taken as [100]. In principle, the (111) plate could have contained equal proportions of [111], [1$\bar{1}$1], [$\bar{1}$11] and [$\bar{1}\bar{1}$1] domains with a complex pattern of twin walls. In practice, the stress imposed by loading of the GHz probe would have favoured twins with the $\bar{3}$ axis parallel to the travel direction (i.e. [111], twin I) since there is a small negative spontaneous strain in this direction, due to the $Pm\bar{3}m \leftrightarrow R\bar{3}c$ transition, and a positive strain in the plane perpendicular to it. In terms of the orientations discussed above, this would give a travel direction of [111] through the [111] twin.

Echoes from shear waves were not detected other than from a 100 μm thick (110) plate. This had twin wall traces aligned parallel to [1$\bar{1}$0]. When the polarization direction was perpendicular to the twin wall traces, no echoes were detected. When the polarization direction was parallel to them, an adequate signal was obtained. This experiment corresponds as nearly as possible to determination of the velocity through a single twin for a shear wave travelling in the [110] direction with polarization parallel to [1$\bar{1}$0].

Experimentally determined velocities, together with other experimental details are listed in table 2. These were converted to elastic moduli using the room temperature density, 6.52 g cm^{-3}, quoted above. The single crystal moduli which make up the effective elastic moduli for the relevant travel directions are included in table 3.

6.2. Brillouin spectroscopy

Spectra collected round the chi circle for the (110) and (100) plates are shown in figure 4 and velocities from the peak positions are shown in figure 5. Data for the (110) plate include spectra collected before and after the first heating and cooling cycle described by Carpenter *et al* (2010c), during which the crystal was heated above the $Pm\bar{3}m \leftrightarrow R\bar{3}c$ transition temperature. There is symmetry in the velocity variations about the [1$\bar{1}$0] and [001] directions in the (110) plate and about [001], [011] and [01$\bar{1}$] in the (100) plate. The (110) plate contains [1$\bar{1}$1] and [1$\bar{1}\bar{1}$] directions, and the observed symmetrical pattern is consistent with a type I twin ($\bar{3}$ axis ∥ [111]), with or without type IV twins ($\bar{3}$ axis ∥ [$\bar{1}\bar{1}$1]) sharing (110), as shown in figure 2. Peaks corresponding to one LA-wave and two TA-waves, TA_1 and TA_2, are present in every direction within the (110) plate and no further peaks arising from alternative twin orientations can be seen. Spectra from the (100) plate also each contain strong peaks consistent with one LA-wave and two TA-waves, but the symmetric distribution of these is not consistent with the symmetry around [001] of a single $\bar{3}m$ twin. The (100) plane in a [111] twin has [011] within a mirror and [0$\bar{1}$1] parallel to a diad (figure 2). Additional weak LA-wave peaks are clearly present in spectra from specific orientations, however, as indicated by arrows in figure 4(b) and by open circles in figure 5(b), and some of the strong TA-wave peaks appear to be broader than others. This is interpreted as indicating that two or more twins were sampled in the experiment, with the diad direction of one twin superimposed on the direction containing a mirror plane in the other, while crystallographic directions of the form [001] and [010] are the same for both twins. Velocities for the LA-waves of these twins are sufficiently different in some directions to give separate peaks while the TA-wave velocities are presumed to be sufficiently similar that their peaks overlap.

Single crystal moduli for crystal class $\bar{3}m$ were obtained first by fitting to the LA- and TA-wave data from the (110) and (100) plates separately. These were in close agreement. The final 'best fit' data were obtained by fitting to velocities from both plates simultaneously. The quality of the fit between

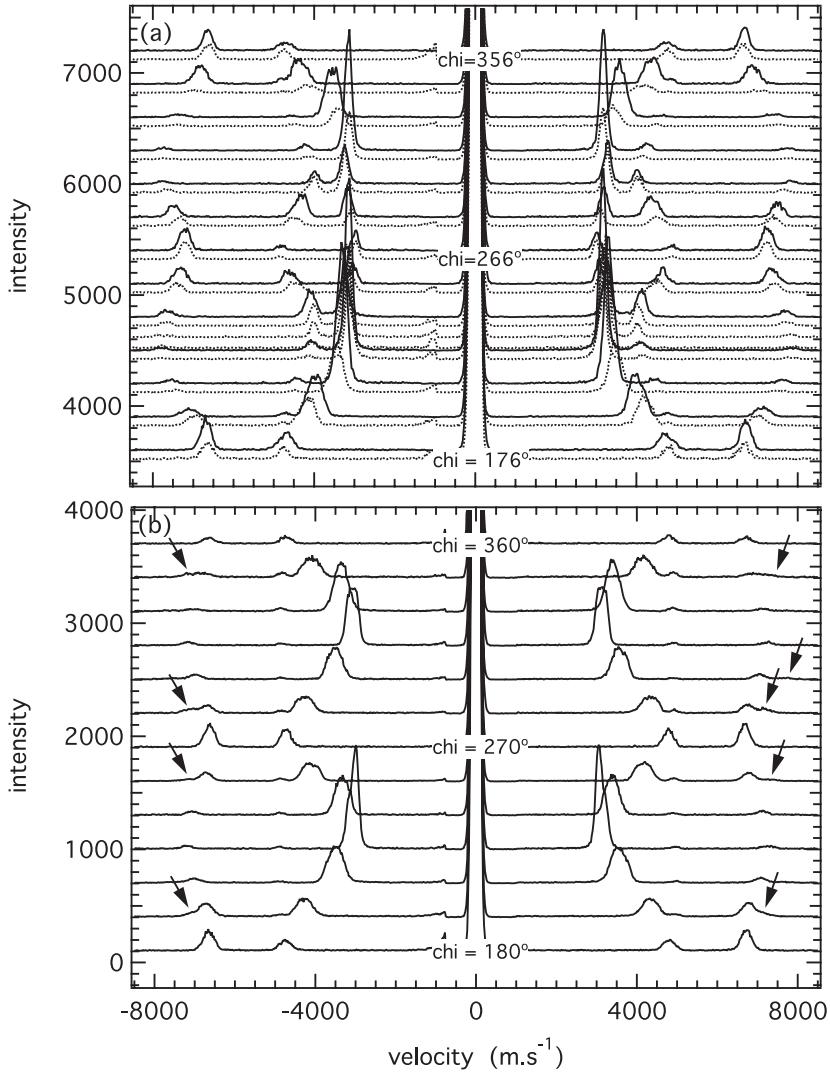

Figure 4. Brillouin spectra collected at room temperature round the chi circle (i.e. for acoustic phonon travel directions within the plane of the plate) for (a) a (110) plate and (b) a (100) plate. Spectra collected before heating are shown as solid lines; spectra collected after the first heating cycle to high temperatures (Carpenter *et al* 2010c) are shown as dotted lines. The spectra have been shifted up the *y* axis according to the chi angle within the crystal plate at which they were collected. Three peaks are seen in spectra from the (110) plate (LA, TA_1, TA_2). Additional LA-wave peaks are evident in selected spectra from the (100) plate, as indicated by arrows. Some of the TA-wave peaks in spectra from the (100) plate appear to be broader than others; this is interpreted as being due to overlapping peaks from acoustic phonons in at least two different twins.

observed and calculated variations is shown in figure 5 and the resulting moduli are listed in table 4, for both trigonal and cubic reference axes. Corresponding velocities for a second twin in the (100) plate were obtained by setting the diad axis parallel to [011] with [$0\bar{1}1$] in the mirror plane (figure 2). These are shown as broken lines in figure 5(b), and the two sets of velocities together give the apparent symmetry about [001]. The rms error from fitting to 62 data points was 1.0%. This is interpreted to imply uncertainties of $\pm\sim1\%$ for diagonal terms of the trigonal elastic modulus matrix and ±2–3% for off-diagonal terms.

7. Discussion

Notwithstanding the inherent difficulties associated with determining phonon travel directions for data collected from crystals containing intimate intergrowths of transformation twins, a unique set of single crystal moduli has been obtained for $LaAlO_3$ at room temperature. These are internally consistent for observations made by two independent experimental methods, and have been compared with calculated values by Luo and Wang (2008a). The GHz pulse-echo ultrasonic measurements were, in effect, made for travel directions which are perpendicular to the phonon travel directions examined by Brillouin spectroscopy. The degree of internal consistency is illustrated in figure 5, which includes velocities for directions within the (110) and (100) plates that are related by symmetry to the directions in which the GHz measurements were actually made. Combinations of moduli which determine the LA- and TA-wave velocities for selected crystallographic directions are listed in table 3, together with their actual values calculated from the 'best fit' data set given

Table 5. Room temperature values from the literature for the bulk (K) and shear (G) moduli of aluminate perovskites. 'EoS' refers to data obtained by fitting an equation of state to lattice parameter data obtained by diffraction from a sample held in a diamond anvil cell at room temperature. Note that data in the early work of Liebermann *et al* (1977) have generally been revised upwards in later studies.

	Source	K (GPa)	G (GPa)
$LaAlO_3$, $R\bar{3}c$	Bouvier and Kreisel (2002) EoS	190 ± 5	
$LaAlO_3$, $R\bar{3}c$	Zhao *et al* (2004) EoS	177 ± 4	
$LaAlO_3$, $R\bar{3}c$	This study, Brillouin	196	105
$PrAlO_3$, $R\bar{3}c$	Kennedy *et al* (2002) in Zhao *et al* (2004) EoS	205 ± 8	
$ScAlO_3$, *Pnma*	Liebermann *et al* (1977) Pulse-echo at 0.6 GPa, 3.4% porosity	232 ± 15	101 ± 4
$ScAlO_3$, *Pnma*	Bass (1984) Brillouin	249 ± 13	140 ± 6
$ScAlO_3$, *Pnma*	Ross (1998) EoS	218 ± 1	
$ScAlO_3$, *Pnma*	Kung *et al* (2000) Pulse-echo, 0.5% porosity	219 ± 1	129 ± 0.1
$ScAlO_3$, *Pnma*	Kung *et al* (2000) Pulse-echo, 1.7% porosity	216 ± 1	126 ± 0.1
$YAlO_3$, *Pnma*	Liebermann *et al* (1977) Pulse-echo at 0.6 GPa, 4.9% porosity	204 ± 15	112 ± 4
$YAlO_3$, *Pnma*	Ross (1996) EoS	205 ± 3	
$EuAlO_3$, *Pnma*	Liebermann *et al* (1977) Pulse-echo at 0.6 GPa, 2.4% porosity	203 ± 15	114 ± 5
$EuAlO_3$, *Pnma*	Kung and Rigden (1999) Pulse-echo, sample of Liebermann *et al* (1977) corrected for porosity	213	123
$GdAlO_3$, *Pnma*	Liebermann *et al* (1977) Pulse-echo at 0.6 GPa, 1.6% porosity	179 ± 15	120 ± 5
$GdAlO_3$, *Pnma*	Bass (1984) Brillouin	203 ± 4	120 ± 3
$SmAlO_3$, *Pnma*	Liebermann *et al* (1977) Pulse-echo at 0.6 GPa, 2.2% porosity	178 ± 14	111 ± 4
$SmAlO_3$, *Pnma*	Bass (1984) Brillouin	198 ± 4	123 ± 3

in table 4. The GHz LA-wave result for the (111) plate (412 ± 10 GPa) corresponds within experimental uncertainty to C_{33T} (411.2 GPa), as expected for a single [111] twin. The GHz results for LA-waves travelling parallel to [110] (408 ± 4) and [100] (295 ± 3 GPa) are also close to the calculated values (397.3 and 289.8 GPa, respectively). The only shear wave which could be detected in the GHz experiments corresponds to $\frac{1}{2}(C_{11} - C_{12})$ and the GHz value (64 ± 1 GPa) is again close to the calculated value (68.3 GPa). Interestingly, shear waves which could not be detected in (111), (110) and (100) plates all depend to some extent on C_{44}, and will have involved stresses within the crystals which could have caused twin wall motion. It is possible, therefore, that the difficulty encountered in obtaining shear wave echoes could have been due to a degree of anelastic dissipation or scattering by the twin walls.

The Voigt–Reuss–Hill value of the adiabatic bulk modulus obtained in the present study (196 GPa) agrees more closely with the isothermal value given by Bouvier and Kreisel (2002) (190 ± 5 GPa) than with the value given by Zhao *et al* (2004) (177 ± 4). Both the latter are from equation of state (EoS) fits to lattice parameter data obtained using x-ray diffraction from a single crystal held within a diamond anvil cell. The EoS bulk modulus of $PrAlO_3$, which also has $R\bar{3}c$ symmetry at room temperature, is 205 ± 8 GPa (data of Kennedy *et al* 2002, as analysed by Zhao *et al* 2004). There appear to be no previously published data for the shear modulus of aluminate perovskites with $R\bar{3}c$ symmetry at room pressure and temperature. Quite a number of studies have been undertaken on aluminate perovskites with *Pnma* symmetry, however, and bulk elastic properties of these are summarized in table 5. The earlier work of Liebermann *et al* (1977) has, by and large, been superceded by more recent studies which report larger values of K and G than found for $LaAlO_3$. EoS values of K overlap with Brillouin data and the more recent pulse-echo ultrasonic values. They cluster in the range ~200–215 GPa for $ScAlO_3$, $EuAlO_3$, $GdAlO_3$, $SmAlO_3$ and $YAlO_3$. An equivalent selection of data puts G for $ScAlO_3$, $EuAlO_3$, $GdAlO_3$ and $SmAlO_3$ in the range 120–130 GPa. There will, of course, be variations due to density and bond strengths, but the relatively lower values of K and G for $LaAlO_3$, 196 and 105 GPa, are consistent with the unexpected result that the *Pnma* structures of (Ca, Sr)TiO_3 and $SrZrO_3$ are elastically stiffer than their $I4/mcm$ structures (Carpenter *et al* 2007, McKnight *et al* 2009). This is counter

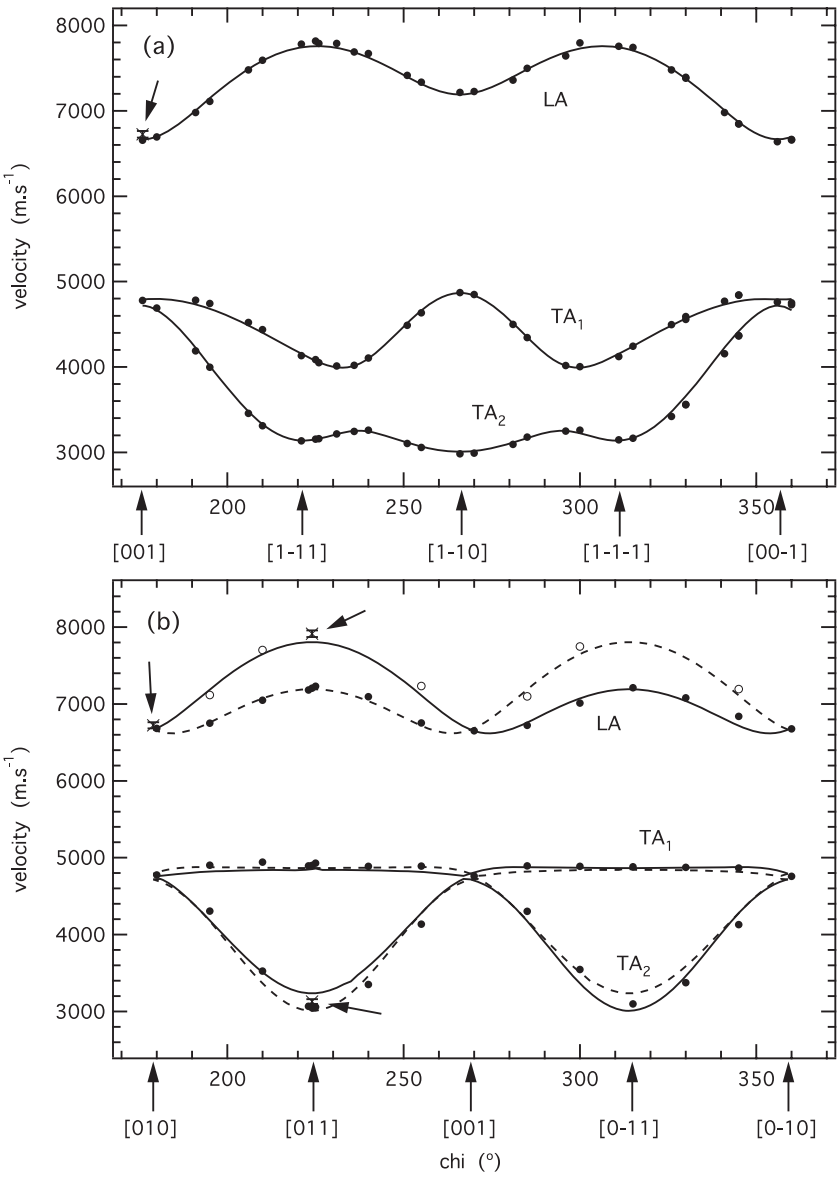

Figure 5. Velocity data extracted from the room temperature Brillouin spectra shown in figure 4: (a) (110) plate, (b) (100) plate. Crystallographic directions refer to the cubic reference axes shown in figure 3. Solid lines represent calculated velocities obtained by fitting to LA, TA_1 and TA_2 velocity data from both plates simultaneously for a type I twin. For this fitting process, it was assumed that velocities for the faster of the LA-waves in directions between [010] and [001] and velocities for the slower LA-waves in directions between [001] and [0$\bar{1}$0] belong to twin I. The second set of LA-wave velocities then corresponds to the second possible twin orientation. Calculated velocities for the latter are shown as broken lines. Note that peaks from LA-waves of the two twin orientations would overlap in the Brillouin spectra. Data for ultrasonic velocities (crosses with error bars, also indicated by arrows) are shown for orientations which are related by symmetry to those from which the GHz data were collected.

to expectation because displacive transitions generally result in elastic softening due to classical strain/order parameter coupling (Slonczewski and Thomas 1970, Rehwald 1973, Lüthi and Rehwald 1981, Carpenter and Salje 1998). It appears that instabilities associated with the R-point only, giving $R\bar{3}c$, $Imma$ or $I4/mcm$ structures, result in classical softening while the subsequent addition of an M-point instability, to give the $Pnma$ structure, causes stiffening. McKnight *et al* (2009) have speculated that this could be a consequence of geometrical constraints such that the deformed octahedra of $Pnma$ structures are impeded from rotating around their usual tilt axes when an external stress is applied.

If the differences in elastic properties between $R\bar{3}c$ (or $Imma$, $I4/mcm$) and $Pnma$ structures are a general feature of tilted perovskites, there might be implications for the mechanisms and influence of coupling with other driving mechanisms for phase transitions. For example, ferroelectric displacements or Jahn–Teller distortions might couple strongly with octahedral tilting in a perovskite with one tilt system but not in a perovskite which has both R- and M-point tilts. For the present, the newly determined elastic properties of $LaAlO_3$ at room temperature form the starting point of a detailed investigation of the direct influence of the $Pm\bar{3}m \leftrightarrow R\bar{3}c$ transition at higher temperatures (Carpenter *et al* 2010c,

2010a). These moduli will also provide a point of reference in studies of elastic relaxations between thin films and single crystal $LaAlO_3$ substrates.

Acknowledgments

Elasticity measurements on $LaAlO_3$ have been supported by The Natural Environment Research Council of Great Britain, first under grant no. NER/A/S/2000/01055 and subsequently under grant no. NE/B505738/1 (to MAC). SDJ acknowledges support from the US National Science Foundation grant EAR-0748707 and the David and Lucile Packard Foundation. JDB acknowledges support from the US National Science Foundation through grants EAR 0135642 and 0738871.

References

Bass J D 1984 *Phys. Earth Planet. Inter.* **36** 145–56
Bouvier P and Kreisel J 2002 *J. Phys.: Condens. Matter* **14** 3981–91
Bueble S, Knorr K, Brecht E and Schmahl W W 1998 *Surf. Sci.* **400** 345–55
Carpenter M A, Buckley A, Taylor P A and Darling T W 2010a *J. Phys.: Condens. Matter* **22** 035405
Carpenter M A, Buckley A, Taylor P A, McKnight R E A and Darling T W 2010b *J. Phys.: Condens. Matter* **22** 035406
Carpenter M A, Li B and Liebermann R C 2007 *Am. Mineral.* **92** 344–55
Carpenter M A and Salje E K H 1998 *Eur. J. Mineral.* **10** 693–812
Carpenter M A, Sinogeikin S V and Bass J D 2010c *J. Phys.: Condens. Matter* **22** 035404
Chrosch J and Salje E K H 1999 *J. Appl. Phys.* **85** 722–7
Delugas P, Fiorentini V and Filippetti F 2005 *Phys. Rev.* B **71** 134302
Harrison R J and Redfern S A T 2002 *Phys. Earth Planet. Inter.* **134** 253–72
Harrison R J, Redfern S A T, Buckley A and Salje E K H 2004a *J. Appl. Phys.* **95** 1706–17
Harrison R J, Redfern S A T and Salje E K H 2004b *Phys. Rev.* B **69** 144101
Hayward S A, Morrison F D, Redfern S A T, Salje E K H, Scott J F, Knight K S, Tarantino S, Glazer A M, Shuvaeva V, Daniel P, Zhang M and Carpenter M A 2005 *Phys. Rev.* B **72** 054110
Hayward S A, Redfern S A T and Salje E K H 2002 *J. Phys.: Condens. Matter* **14** 10131–44
Jacobsen S D, Reichmann H J, Kantor A and Spetzler H 2005 *Advances in High-Pressure Technology for Geophysical Applications* ed J Chen, Y Wang, T S Duffy, G Shen and L P Dobrzhinetskaya (Amsterdam: Elsevier) p 25
Jacobsen S D, Reichmann H-J, Spetzler H A, Mackwell S J, Smyth J R, Angel R J and McCammon C A 2002 *J. Geophys. Res.* **107** doi:10.1029/2001JB000490
Kantor A P, Jacobsen S D, Kantor I Yu, Dubrovinsky L S, McCammon C A, Reichmann H J and Goncharenko I N 2004 *Phys. Rev. Lett.* **93** 215502
Kennedy B J, Vogt T, Martin C D, Parise J B and Hriljac J A 2002 *Chem. Mater.* **14** 2644–8
Kung J and Rigden S 1999 *Phys. Chem. Miner.* **26** 234–41
Kung J, Rigden S and Gwanmesia G 2000 *Phys. Earth Planet. Inter.* **118** 65–75
Lee A E, Platt C E, Burch J F, Simon R W, Goral J P and Al-Jassim M M 1990 *Appl. Phys. Lett.* **57** 2019–21
Lehmann A G, Sanna C, Lampis N, Congiu F, Concas G, Maritato L, Aruta C and Petrov A Yu 2007 *Eur. Phys. J.* B **55** 337–45
Liebermann R C, Jones L E A and Ringwood A E 1977 *Phys. Earth Planet. Inter.* **14** 165–78
Liu P F and Jiang Q 2006 *Phys. Lett.* A **352** 451–6
Luo X and Wang B 2008a *J. Appl. Phys.* **104** 073518
Luo X and Wang B 2008b *J. Appl. Phys.* **104** 053503
Lüthi B and Rehwald W 1981 *Topics in Current Physics* vol 23, ed Müller K A and H Thomas (Berlin: Springer) pp 131–84
Masuno A, Haruta M, Azuma M, Kurata H, Isoda S, Takano M and Shimakawa Y 2006 *Appl. Phys. Lett.* **89** 211913
Masuno A, Terashima T, Shimakawa Y and Takano M 2004 *Appl. Phys. Lett.* **85** 6194–6
McKnight R E A, Howard C J and Carpenter M A 2009 *J. Phys.: Condens. Matter* **21** 015901
Nye J F 1985 *Physical Properties of Crystals* (Oxford: Oxford University Press)
Palko J W, Sayir A, Sinogeikin S V, Kriven W M and Bass J D 2002 *J. Am. Ceram. Soc.* **85** 2005–12
Peacock P W and Robertson J 2002 *J. Appl. Phys.* **92** 4712–21
Phillips J M 1996 *Appl. Phys. Rev.* **79** 1829–48
Rehwald W 1973 *Adv. Phys.* **22** 721–55
Ross N L 1996 *Phase Transit.* **58** 27–41
Ross N L 1998 *Phys. Chem. Miner.* **25** 597–602
Sathe V G and Dubey A 2007 *J. Phys.: Condens. Matter* **19** 382201
Schilling F R, Sinogeikin S V and Bass J D 2003 *Phys. Earth Planet. Inter.* **136** 107–18
Shevlin S A, Curioni A and Andreoni W 2005 *Phys. Rev. Lett.* **94** 146401
Simon R W, Platt C E, Lee A E, Lee G S, Daly K P, Wire M S, Luine J A and Urbanik M 1988 *Appl. Phys. Lett.* **53** 2677–9
Sinogeikin S V, Katsura T and Bass J D 1998 *J. Geophys. Res.* **103** 20819–25
Slonczewski J C and Thomas H 1970 *Phys. Rev.* B **1** 3599–608
Spetzler H A, Chen G, Whitehead S and Getting I C 1993 *Pure Appl. Geophys.* **141** 341–77
Vali R 2008 Phonons and heat capacity of $LaAlO_3$ *Comput. Mater. Sci.* **44** 779–82
Walsh J N, Taylor P A, Buckley A, Darling T W, Schreuer J and Carpenter M A 2008 *Phys. Earth Planet. Inter.* **167** 110–7
Xiang W, Lü H, Yan L, Guo H, Liu L, Zhou Y, Yang G, Jiang J, Cheng H and Chen Z 2003 *J. Appl. Phys.* **93** 533–6
Xiong K, Robertson J and Clark S J 2006 *Appl. Phys. Lett.* **89** 022907
Zhao J, Ross N L and Angel R J 2004 *J. Phys.: Condens. Matter* **16** 8763–73
Zhu J, Liang Z, Li Y R, Zhang Y and Wei X H 2006 *J. Cryst. Growth* **294** 236–42